# Numerical Modelling of Tumor Transport in Fluid Flows

Ahmed, Meraj; Nguyen, Tam Thien; Akerkouch, Lahcen; Tavasso, Margherita; Bordoloi, Ankur Deep; Le, Trung B.

**DOI**
10.1115/DMD2025-1060

**Publication date**
2025

**Document Version**
Final published version

**Published in**
Proceedings of the 2025 Design of Medical Devices Conference, DMD 2025

**Citation (APA)**
Ahmed, M., Nguyen, T. T., Akerkouch, L., Tavasso, M., Bordoloi, A. D., & Le, T. B. (2025). Numerical Modelling of Tumor Transport in Fluid Flows. In *Proceedings of the 2025 Design of Medical Devices Conference, DMD 2025* Article V001T02A005 American Society of Mechanical Engineers (ASME). https://doi.org/10.1115/DMD2025-1060

Proceedings of the 2025 Design of Medical Devices Conference
DMD2025
April 28-30, 2025, Minneapolis, MN, USA

DMD2025-1060

# NUMERICAL MODELLING OF TUMOR TRANSPORT IN FLUID FLOWS

**Meraj Ahmed**
Department of Civil, Construction, and Environmental Engineering, North Dakota State University

**Tam Thien Nguyen**
Department of Civil, Construction, and Environmental Engineering, North Dakota State University

**Lahcen Akerkouch**
Department of Civil, Construction, and Environmental Engineering, North Dakota State University

**Margherita Tavasso**
Department of Chemical Engineering, Delft University of Technology, Delft, 2629 HZ The Netherlands

**Ankur Deep Bordoloi**
Department of Chemical Engineering, Delft University of Technology, Delft, 2629 HZ The Netherlands

**Trung B. Le**
Department of Civil, Construction, and Environmental Engineering, North Dakota State University



## ABSTRACT

*Cancer metastasis leads to the transport and widespread of malignant cells from the primary tumor to other parts of the body by exploiting body fluids (lymphatic fluid, bloodstream, and interstitial fluid). While the transport of a single cancer cell in fluid flow has been studied in the past, it is unclear how a group of cancer cells (tumor) migrate under the impact of hydrodynamic force in vasculature. In this work, we address this knowledge gap by investigating the migration process of a cancer spheroid tumor in a micro-channel with a constriction using both experimental and computational methods. The Dissipative Particle Dynamics method was employed to simulate the mechanical components of the spheroid tumor and immersed boundary method is used for interaction of spheroid with the surrounding fluid. Our results suggest that the mechanical response of the spheroid tumor differs from a single cell. Our computational framework provides new capabilities for designing bioengineering devices for cell manipulation.*

Keywords: metastasis, transport, cancer cells, micro-channel, Dissipative Particle Dynamics, immersed boundary method.

## 1 INTRODUCTION

Cancer metastasis leads to the transport and widespread of malignant cells from the primary tumor to other parts of the body by exploiting body fluids (lymphatic fluid, bloodstream, and interstitial fluid) [1]. The metastasis process consists of a series of successive actions beginning by: (i) invasion of the primary tumor in the surrounding tissue; (ii) intravasation into the surrounding vasculature or lymphatic system; (iii) survival in the circulation ; and (iv) arrest at the new location. Finally, the cancer cell extravases and colonizes to the secondary tumor site [2]. While this process has been known in general, the detailed mechanism of cancer metastasis is not known, especially the impact of hydrodynamic force on the metastasis. For example, Byrd et al. [3] generated three-dimensional tumor models based on MRI images obtained from various breast cancer patients. Their results showed that breast cancers were categorized into four main distinct tumor shapes: discoidal, segmental, spherical and irregular. These shapes are important as they are the building blocks for the creation of 3D tumors in microvasculature environments.

The physical characteristics of circulating tumor cells (CTCs) that allow them to migrate in different directions and survive under the physiological blood flow is still poorly understood. Numerical methods are found to precisely model the high deformability of CTCs, cell-cell interaction, and interaction with the fluid flow in the microcapillaries [4–7]. These models can be used to find the locations where the next tumor is most likely to form [8].

In most previous literatures the CTCs were modelled as immersed boundaries and the elastic property of the membrane were modelled using Hookean springs [9]. Furthermore, previous models in the literature rely only on particle-based methods to simulate cell and plasma dynamics, which do not report the extracellular flow patterns [2,10,11], as well as the loading condition on the cellular membrane. Lattice-base methods is suitable to model the governing equations of cell-cell interaction, cell-fluid interaction, cell-wall interactions, cell deformation and reaction to microenvironment stimuli [12]. But large length scale variation ranging from cellular scale to organ scale, these methods are not suitable to simulate large complex biological systems. Dissipative Particle Dynamics (DPD) methods are suitable for modelling systems at mesoscale [13]. Both continuum and discrete models play an important role in cancer metastasis. Therefore, hybrid methods are more suitable for modelling such processes. Hybrid methods use both discrete

Corresponding author. e-mail: trung.le@ndsu.edu

representation for cellular scale phenomena and continuum methods for tumor or tissue scale phenomena [14].

In the present research the cancer tumor is represented by a sphere. The surface of sphere is modeled as a viscoelastic shell composed of DPD particles connected by viscoelastic springs and the resistance offered by the cancer cells inside the tumor are modelled by free DPD particles [15]. The effect of surrounding fluid on the tumor has not been modelled in the present study. Our future goal is to use immersed boundary-based continuum method to include the effect of surrounding fluid on the tumor. Our method demonstrates its applicability in simulating transport of tumors in capillary channels.

## 2 MATERIALS AND METHODS

### 2.1 GEOMETRY

Figure 1a shows the dimensions of the micro channel with constriction. All the dimensions are in microns. Figure 1b shows the three-dimensional view of the micro channel. The micro channel is modelled as a rigid wall and no slip boundary condition has been applied on the inner wall surface. A sphere has been used to represent the tumor, as shown in Figure 1c. The diameter of the sphere is 286.0 microns.

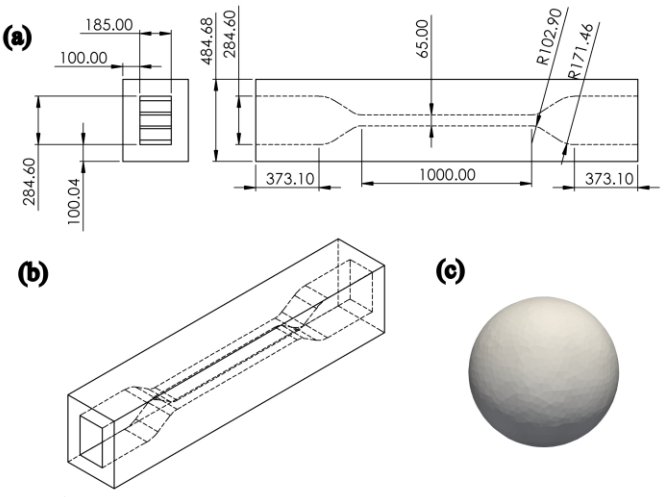


*Figure 1. (a) Design dimensions (microns) of the microchannel with constriction, (b) three-dimensional view of the micro channel, (c) the spherical model of the lump of cancer cell.*

### 2.2 EXPERIMENTAL SETUP

Figure 2 shows the experimental apparatus at the Department of Chemical Engineering, Delft University of Technology. The details of the experimental apparatus are adapted from [16]. The sphere consisting of cancer cells is forced to pass through a constricted micro channel with the help of fluid flowing in the channel, as shown in Figure 2. The cross section of the channel is usually made rectangular to accommodate the irregular shape of tumor. A high-speed camera is used to capture the displacement and deformation of the sphere while it passes through the channel. With the help of image processing capability of MATLAB, the boundary of the lump of cancer cells were extracted and the engineering strain, which is the ratio of instantaneous length after deformation to the initial length, in the outer surface of the sphere is calculated. This strain is then used to calibrate the DPD model parameters.

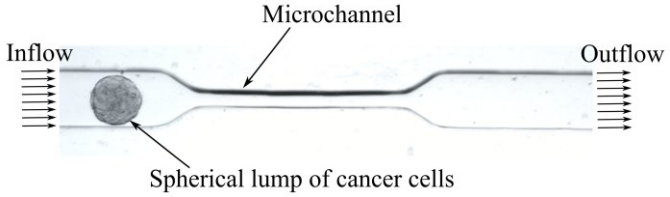


*Figure 2. The snapshot of the experimental setup [16].*

### 2.3 DISSIPATIVE PARTICLE DYNAMICS METHOD

Dissipative Particle Dynamics (DPD) is a particle-based model similar to a coarse-grained molecular dynamics model. The DPD method utilizes the interaction of particles through pairwise forces in order to predict the dynamics of membrane as well as the interacting fluid surrounding the membrane. In DPD method, the particle *i* can interact with the surrounding particle *j* within cutoff radius $r_c$ by: (a) conservative force $F_{ij}^C$, (b) the dissipative force $F_{ij}^D$, (c) the random force $F_{ij}^R$ and the penalty force $F_{ij}^P$. The total force $f_i$ on particle *i* is given by

$$f_i = \sum_{j \neq i} F_{ij}^C + F_{ij}^D + F_{ij}^R + F_{ij}^P \tag{1}$$

The outer surface of the sphere is modelled as a viscoelastic membrane and the resistance offered by the cancer cells inside the sphere is modelled using dissipative particles.

#### 2.3.1 CONSERVATIVE FORCE

The conservative force $F_{ij}^C$ is given by:

$$F_{ij}^C = F^C(r_{ij})\hat{r_{ij}}$$

$$F^C(r_{ij}) = \begin{cases} a_{ij}\left(1 - \dfrac{r_{ij}}{r_c}\right) & for \;\; r_{ij} < r_c \\ 0 & for \;\; r_{ij} > r_c \end{cases} \tag{2}$$

Where $a_{ij} = 20$ is the conservative force coefficient between particles *i* and *j*, and $r_c = 1$ is the cut off radius.

#### 2.3.2 THE DISSIPATIVE FORCE

The dissipative force $F_{ij}^D$ for the membrane particles is given by:

$$F_{ij}^D = -\Gamma^T v_{ij} - \Gamma^C (v_{ij} \cdot \hat{r_{ij}})\hat{r_{ij}} \tag{3}$$

Superscripts C and T denote the central and translational components. $\Gamma^C$ is equal to one third of $\Gamma^T$. Therefore, large portion of viscosity depends on $\Gamma^T$. $v_{ij} = v_i - v_j$ is the relative velocity between particles *i* and *j*.

The physical viscosity of the membrane $\eta_m$ is related to the translational and central viscosity component as following:

$$\eta_m = \sqrt{3}\Gamma^T + \frac{\sqrt{3}\Gamma^C}{4} \quad (4)$$

### 2.3.3 THE RANDOM FORCE

General Fluid particle model [2,15] and membrane viscosity models are used to define the random force $F_{ij}^R$.

$$F_{ij}^R dt = \sqrt{2k_B T}\left(2\sqrt{\frac{2\sqrt{3}}{13}\eta_m}d\overline{W_{ij}^S}\right)\hat{r_{ij}} \quad (5)$$

Where $dt$ is the physical time step. $d\overline{W_{ij}^S} = dW_{ij}^S - tr(dW_{ij}^S)/3$, where $tr(dW_{ij}^S)$ is the trace of the random matrix of independent Wiener increments $dW_{ij}$.

### 2.3.4 PENALTY FORCE

The penalty force is used to reflect the particles back whenever they come close to the membrane. The inside or outside the membrane position of the particle can be checked by the following condition:

$$n_i \cdot r_{ij} = \begin{cases} < 0 & inside\ the\ cell \\ > 0 & outside\ the\ cell \end{cases} \quad (6)$$

Where $n_i$ is the normal vector at the membrane and $r_{ij}$ is the relative position vector of the particle.

## 2.4 SHELL MODELING

The cancer tumor is assumed to consist of a thin shell structure in the outer layer and a viscoelastic core. The shell's physical characteristics, such as viscosity, elasticity, and bending stiffness, are derived fundamentally from these biological components. The shell structure is modeled as a spring-network structure. The surface of the shell is discretized using triangular elements. The edges of these triangles are modelled as non-linear viscoelastic springs, while the nodes of the triangles are modelled as DPD particles (Figure 3). The forces between the membrane DPD particles are calculated from potential energy $V(\boldsymbol{r}_i)$ as follows:

$$\boldsymbol{F}_i^{membrane} = \frac{\partial V(\boldsymbol{r}_i)}{\partial \boldsymbol{r}_i} \quad (7)$$

Where $\boldsymbol{r}_i$ is the position vector of the particle. The potential energy of the membrane is a combination of the in-plane ($V_{in-plane}$), bending ($V_{bending}$), area ($V_{area}$), and volume ($V_{volume}$) energy, given by:

$$V(\boldsymbol{r}_i) = V_{in-plane} + V_{bending} + V_{area} + V_{volume} \quad (8)$$

Where $\boldsymbol{r}_i$ is the position vector of the vertices where the potential energy is defined.

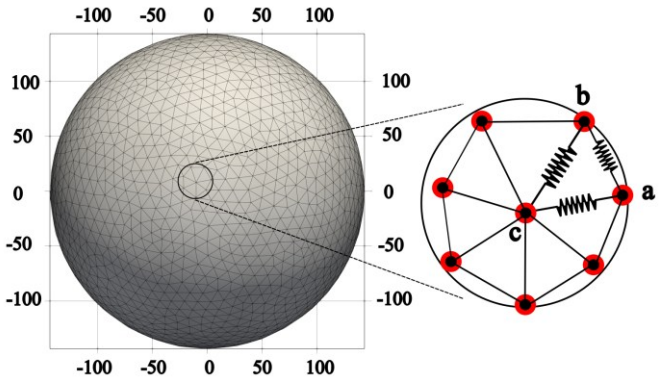


*Figure 3. Triangulated surface of the shell. The red circles are DPD particles, and the edges of the triangles are nonlinear viscoelastic springs as shown in triangle abc.*

The in-plane potential energy term accounts for the elastic energy stored in the shell. Here, the nonlinear wormlike-power (WLC−POW) model is used:

$$V_{in-plane} = \sum_{j\in 1\ldots N_s} U_{WLC}(l_j) + \sum_{k\in 1\ldots N_t} U_{POW}(l_j) \quad (9)$$

The Wormlike Chain (WLC) attractive potentials ($U_{WLC}(l_j)$) for individual links $(l_j)$ is expressed as:

$$U_{WLC}(l_j) = \frac{k_B T l_{max}}{4p}\frac{3x^2 - 2x^3}{1-x} \quad (10)$$

where $l_j$ is the length of the spring $j$, and $x = \frac{l_j}{l_m}$ represents the spring deformation. $l_{max}$, and $p$ is the maximum length of the links and the persistence length, respectively. $k_B$ and T are the Boltzmann's constant and the temperature, respectively.

The energy potential, $U_{POW}$, which defines a repulsive force in the form of a power function (POW). $U_{POW}$ depends on the separation distance $l_j$ as:

$$U_{POW}(l_j) = \frac{k_P}{4(m-2)l_j^{m-1}}, \quad m > 0, m \neq 1 \quad (11)$$

The bending energy $V_{bending}$ is defined as,

$$V_{bending} = \sum_{j\in 1\ldots N_s} k_b[1 - \cos(\theta_j - \theta_0)] \quad (12)$$

Here $k_b$ and $\theta_0$ are the bending constant and the spontaneous angle, respectively. $\theta_j$ is the instantaneous angle between two adjacent triangles, which share the common edge (link) j as shown in Figure 4.

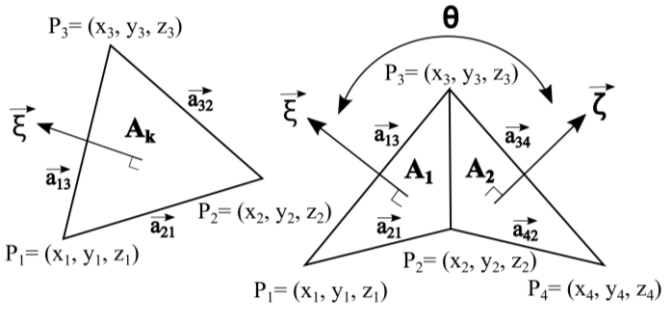


*Figure 4. $P_1$, $P_2$, $P_3$, $P_4$ are the nodes of the triangle and $A_k$ is the area of the triangle. $A_1$ and $A_2$ are the area of the two adjacent triangles. $a_{21}$, $a_{32}$, $a_{13}$, $a_{34}$, $a_{42}$ are the position vectors along the edges of the triangle. $\xi$ and $\zeta$ are the unit normal vectors to the area of the triangles. $\theta$ is the angle between the unit normal vectors $\xi$ and $\zeta$.*

The area and volume conservation constraints account for the incompressibility of the shell and the core, respectively. They are defined as:

$$V_{area} = \frac{k_a(A - A_0^{tot})^2}{2A_0^{tot}} + \sum_{k\in 1\ldots N_t} \frac{k_d(A_k - A_0)}{2A_0} \tag{13}$$

$$V_{volume} = \frac{k_v(V - V_0^{tot})^2}{2V_0^{tot}} \tag{14}$$

Where $A_k$ and $A_0$ are the instantaneous areas of the $k^{th}$ triangle (element) and the average area per element. $k_a$, $k_d$, and $k_v$ are the global area, local area, and volume constraint coefficients, respectively. $A$ and $V$ are the instantaneous total area and total volume of the lump. The $A_0^{tot} = N_t A_0$ and $V_0^{tot}$ are the specified total area and volume, respectively.

## 2.5 CELL VISCOSITY

The cancer cell is viscoelastic in nature. The membrane viscosity contribution is expressed as an additionally dissipative force as given in equation 3. The nodes of the triangular elements used to discretize the membrane are modelled as DPD particles. There are 1940 DPD particles used to model the membrane of the lump.

## 2.6 SCALING OF MODEL AND PHYSICAL UNITS

One challenge in DPD modeling is the relationship between the modeled quantities and the physical value since this relationship is not explicit. It is necessary to use a scaling argument to recover this relationship. Here, the superscript M and P correspond to the model and physical units (SI units), respectively.

The length scale ($r^M$) is defined as:

$$r^M = \frac{D_0^P}{D_0^M} \tag{15}$$

$r^M$ is the model unit of length. Explicitly, $D_0^M$ is the cell diameter in the model unit and $D_0^P$ is the physical cell diameter in meters. The energy per unit mass($k_BT$) and the force N scaling values are given by:

$$(k_BT)^M = \frac{Y^P}{Y^M}\left(\frac{D_0^P}{D_0^M}\right)^2 (k_BT)^P \tag{16}$$

$$N^M = \frac{Y^P}{Y^M}\frac{D_0^P}{D_0^M} N^P \tag{17}$$

Where Y is the membrane Young's modulus. The timescale $\tau$ is defined as follows.

$$\tau = \left(\frac{D_0^P}{D_0^M}\frac{\eta_m^P}{\eta_m^M}\frac{Y^M}{Y^P}\right)^{\alpha} \tag{18}$$

## 2.7 COMPUTATIONAL SETUP

*Table 1. Parameters for DPD model.*

| Parameter | Value | Parameter | Value |
|---|---|---|---|
| $kB$ | $1.38 \times 10^{-23}$[J/K] | $u_0$ | $6.3\times 10^{-6}[N/m]$ |
| $T$ | 23 + 273.15[K] | $x_0$ | 1/2.2 |
| $D_0$ | $286\times 10^{-6}$[m] | $m$ | 2 |
| $\eta_o$ | $1.2\times 10^{-3}$[N.s/m$^2$] | $k_b$ | $2k_c/\sqrt{3}$ |
| $\eta_i$ | $5\eta_o$ | $\theta_0$ | $\cos^{-1}\left(\frac{(\sqrt{3}(N_v-2)-5\pi)}{(\sqrt{3}(N_v-2)-3\pi)}\right)$ |
| $\eta_m$ | $5.1 \times 10^{-2}[N.s/m^2]$ | $D_0^M$ | 286.07 |
| $\eta_m^M$ | $400\eta_m$ | $Y_0^M$ | 400 |
| $N_t$ | $2N_v - 4$ | $k_a$ | $6.17\times 10^{-5}$ |
| $k_c$ | $3.6\times 10^{-15}$[J] | $k_d$ | $1.26\times 10^{-5}$ |
| | | $k_v$ | 836.18 |
| $N_s$ | $3N_t/2$ | $r^M$ | $D_0/D_0^M$ |
| $A_0$ | $4\pi D_0^2/(4N_t)$[m$^2$] | $(kB)^M$ | $(Y/Y_0^M)(D_0/D_0^M)^2$ |
| $L_0^{eff}$ | $\sqrt{4A_0/\sqrt{3}}$ [m] | $N^M$ | $(kB)^M/r^M$ |
| $u_p$ | $2u_0$ | $K$ | $u_p/(4u_p - Y)$ |
| $Y$ | $3.92453u_p$ | | |

The surface of the sphere was discretized using 3876 triangular elements and 1940 nodes or vertices. The nodes are treated as DPD particles, and the edges of the triangles are treated as nonlinear viscoelastic springs. A constant compressive force of 2000 pico-Newton [16] is applied from X and Y directions, While the sphere is free to elongate in the Z direction. In this preliminary study the parameters given in Table 1 have been used for DPD modelling.

## 3 RESULTS AND DISCUSSION

The images of the experiment were used to calculate the engineering strain in the shell (outer surface of the tumor) as it passes through the micro channel. The boundary of the tumor is extracted from the images and ten equidistant points are placed on the boundary of the sphere as shown in Figure 5. As the sphere deforms, the distance between these points also changes

uniformly. Which is then used to calculate the strain in the shell as shown in Figure 6. Note that the shell reaches its terminal shape inside the constriction after 5 seconds.

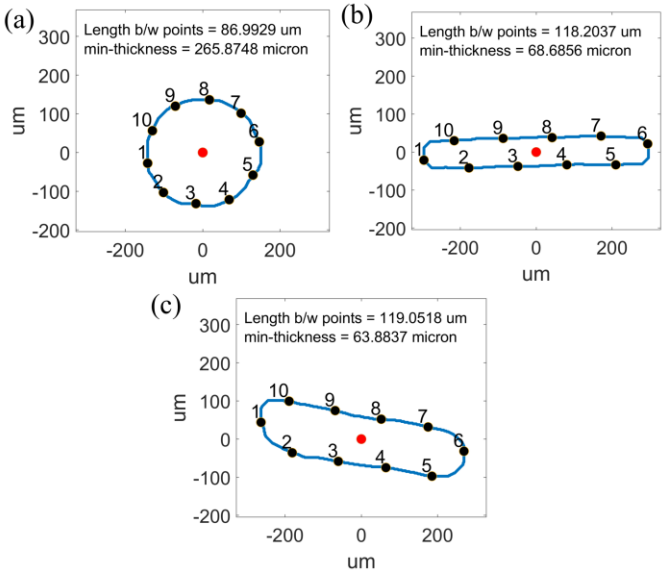


*Figure 5. (a) Equidistant points at t = 0 s, (b) t = 3.0 s, and (c) t = 5.5 s. Units are in microns (um).*

In the beginning of the flow (0 s to 1.0 s) there is a slight decrease in the strain of the shell. After 1 s to 4.8 s the strain increases linearly. After 4.8 s the strain becomes constant. In the beginning of the entry of the tumor into the microchannel (1 s to 1.8 s), the rate of increase of strain is higher than after complete entry of the tumor into the microchannel (1.8 s to 4.3 s). Similarly, when the tumor starts to exit (4.8 s) from the microchannel, the rate of increase of the strain again becomes greater than that during complete entry into the channel.

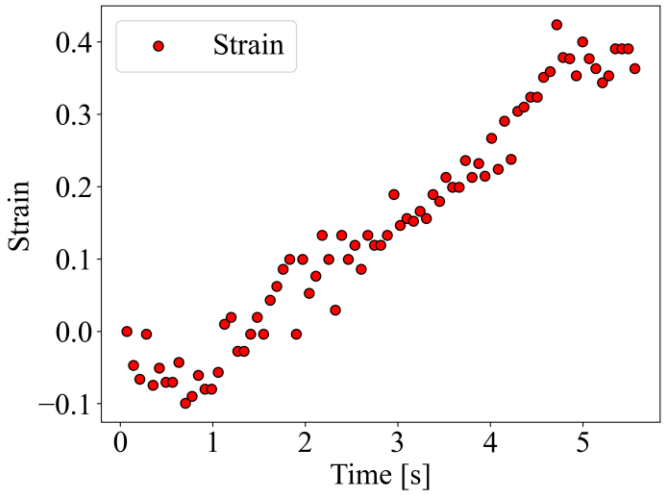


*Figure 6. Variation of circumferential strain in the boundary of the sphere with time.*

Figure 7 shows the comparison of the shapes of the tumor at different times between the experimental and simulation results. It can be observed that the shapes are quite similar in both cases. In the present simulation a constant compressive force has been applied from two directions (X and Y axes) and is left to elongate in the third direction (Z-axis). While in the case of the experiment the force is due to Fluid-Solid-Interaction between the fluid plasma and the tumor as well as the force applied by the wall of the channel. Therefore, the deformed shapes are slightly different in the simulation results as compared to the experimental results.

Therefore, the preliminary results show the potential of the present model to mimic the deformation of the tumor in physiological flow conditions.

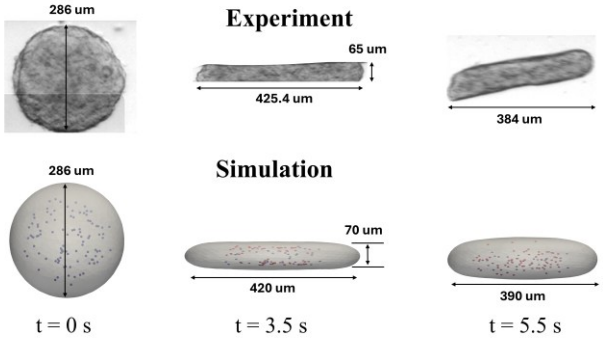


*Figure 7. Comparison of the shapes of the tumor at different time, between experiment and simulation results.*

## 4 CONCLUSION

A computational model using DPD method has been developed to accurately model the response of the tumor of cancer cells subjected to fluid forces. In the current work, constant forces are applied on the surface of tumor to mimic the impact of fluid forces. The mechanics of the tumor is modelled using a separate set of DPD particles. The simulation result show that the deformed shape of the tumor at different times agrees well with one obtained in the corresponding experiment. Therefore, our model is able to mimic the behavior of cancel tumors during their migration through small capillaries.

In this preliminary study, we have not included the fluid solid interaction (FSI) to simulate effect of the surrounding fluid. Our future work is to include the FSI simulation of the tumor, which is essential in understanding hemodynamic loads on tumors during their deformations in capillary vessels.


## ACKNOWLEDGEMENTS

We would like to thank Dr. Pouyan E. Boukany at the Department of Chemical Engineering, Delft University of Technology for his contribution to main ideas of this project. This study is supported by National Science

Foundation Award # 1946202 RII Track-1: ND-ACES: New Discoveries in the Advanced Interface of Computation, Engineering, and Science.

## NOMENCLATURE

| Symbol | Name | Symbol | Name |
|---|---|---|---|
| $kB$ | Boltzmann's constant | $u_0$ | Observed linear elastic shear modulus |
| $T$ | Absolute temperature | $x_0$ | Ratio of spectrin lengths |
| $D_0$ | Diameter | $m$ | Exponent of WLC |
| $k_a$ | Global area coefficient | $k_b$ | Model bending coefficient |
| $\eta_o$ | Blood viscosity | $\theta_0$ | Spontaneous angle |
| $\eta_i$ | Cytoplasm viscosity | $D_0^M$ | Model diameter |
| $\eta_m$ | Membrane viscosity | $Y_0^M$ | Model Young's modulus |
| $\eta_m^M$ | Model membrane viscosity | $k_d$ | Local area coefficient |
| $N_t$ | Number of triangles | $k_v$ | Volume coefficient |
| $k_c$ | Macroscopic membrane bending rigidity | $r^M$ | Length scale factor |
| $N_s$ | Number of sides | | |
| $A_0$ | Surface area | $(kB)^M$ | Model Boltzmann's constant |
| $L_0^{eff}$ | Effective equilibrium length | $N^M$ | Force scaling parameter |
| $u_p$ | Actual elastic shear modulus | $K$ | Bulk modulus |
| $Y$ | Young's modulus | | |

## REFERENCES


[1] Follain, G., Herrmann, D., Harlepp, S., Hyenne, V., Osmani, N., Warren, S. C., Timpson, P., and Goetz, J. G., 2020, "Fluids and Their Mechanics in Tumour Transit: Shaping Metastasis," Nat Rev Cancer, **20**(2), pp. 107–124. https://doi.org/10.1038/s41568-019-0221-x.

[2] Puleri, D. F., Balogh, P., and Randles, A., 2021, "Computational Models of Cancer Cell Transport through the Microcirculation," Biomech Model Mechanobiol, **20**(4), pp. 1209–1230. https://doi.org/10.1007/s10237-021-01452-6.

[3] Byrd, B. K., Krishnaswamy, V., Gui, J., Rooney, T., Zuurbier, R., Rosenkranz, K., Paulsen, K., and Barth, R. J., 2020, "The Shape of Breast Cancer," Breast Cancer Res Treat, **183**(2), pp. 403–410. https://doi.org/10.1007/s10549-020-05780-6.

[4] Keshavarz Motamed, P., and Maftoon, N., 2021, "A Systematic Approach for Developing Mechanistic Models for Realistic Simulation of Cancer Cell Motion and Deformation," Sci Rep, **11**(1), p. 21545. https://doi.org/10.1038/s41598-021-00905-3.

[5] Xiao, L. L., Yan, W. W., Liu, Y., Chen, S., and Fu, B. M., 2018, "Modeling Cell Adhesion and Extravasation in Microvascular System," *Molecular, Cellular, and Tissue Engineering of the Vascular System*, B.M. Fu, and N.T. Wright, eds., Springer International Publishing, Cham, pp. 219–234. https://doi.org/10.1007/978-3-319-96445-4_12.

[6] Dabagh, M., and Randles, A., 2019, "Role of Deformable Cancer Cells on Wall Shear Stress-Associated-VEGF Secretion by Endothelium in Microvasculature," PLoS ONE, **14**(2), p. e0211418. https://doi.org/10.1371/journal.pone.0211418.

[7] Anvari, S., Osei, E., and Maftoon, N., 2021, "Interactions of Platelets with Circulating Tumor Cells Contribute to Cancer Metastasis," Sci Rep, **11**(1), p. 15477. https://doi.org/10.1038/s41598-021-94735-y.

[8] Follain, G., Osmani, N., Azevedo, A. S., Allio, G., Mercier, L., Karreman, M. A., Solecki, G., Garcia Leòn, M. J., Lefebvre, O., Fekonja, N., Hille, C., Chabannes, V., Dollé, G., Metivet, T., Hovsepian, F. D., Prudhomme, C., Pichot, A., Paul, N., Carapito, R., Bahram, S., Ruthensteiner, B., Kemmling, A., Siemonsen, S., Schneider, T., Fiehler, J., Glatzel, M., Winkler, F., Schwab, Y., Pantel, K., Harlepp, S., and Goetz, J. G., 2018, "Hemodynamic Forces Tune the Arrest, Adhesion, and Extravasation of Circulating Tumor Cells," Developmental Cell, **45**(1), pp. 33-52.e12. https://doi.org/10.1016/j.devcel.2018.02.015.

[9] Rejniak, K. A., 2016, "Circulating Tumor Cells: When a Solid Tumor Meets a Fluid Microenvironment," *Systems Biology of Tumor Microenvironment*, K.A. Rejniak, ed., Springer International Publishing, Cham, pp. 93–106. https://doi.org/10.1007/978-3-319-42023-3_5.

[10] Byun, S., Hecht, V. C., and Manalis, S. R., 2015, "Characterizing Cellular Biophysical Responses to Stress by Relating Density, Deformability, and Size," Biophys J, **109**(8), pp. 1565–1573.

[11] Chen, M. B., Whisler, J. A., Fröse, J., Yu, C., Shin, Y., and Kamm, R. D., 2017, "On-Chip Human Microvasculature Assay for Visualization and Quantification of Tumor Cell Extravasation Dynamics," Nat Protoc, **12**(5), pp. 865–880. https://doi.org/10.1038/nprot.2017.018.

[12] Cristini, V., and Lowengrub, J., 2010, *Multiscale Modeling of Cancer: An Integrated Experimental and Mathematical Modeling Approach*, Cambridge University Press. https://doi.org/10.1017/CBO9780511781452.

[13] Moeendarbary, E., Ng, T. Y., and Zangeneh, M., 2009, "DISSIPATIVE PARTICLE DYNAMICS: INTRODUCTION, METHODOLOGY AND COMPLEX FLUID APPLICATIONS — A REVIEW," Int. J. Appl. Mechanics, **01**(04), pp. 737–763. https://doi.org/10.1142/S1758825109000381.

[14] Cristini, V., and Lowengrub, J., 2010, *Multiscale Modeling of Cancer: An Integrated Experimental and Mathematical Modeling Approach*, Cambridge University Press. https://doi.org/10.1017/CBO9780511781452.

[15] Fedosov, D. A., 2010, *Multiscale Modeling of Blood Flow and Soft Matter*, Brown University.

[16] Tavasso, M., Bordoloi, A. D., Tanré, E., Dekker, S. A. H., Garbin, V., and Boukany, P. E., 2024, "Linking Metastatic Potential and Viscoelastic Properties of Breast Cancer Spheroids via Dynamic Compression and Relaxation in Microfluidics," Adv Healthcare Materials, p. 2402715.